J|A|C|S
ARTICLES
Published on Web 05/17/2003

MLCT State Structure and Dynamics of a Copper(I) Diimine Complex Characterized by Pump−Probe X-ray and Laser Spectroscopies and DFT Calculations

Lin X. Chen,*,† George B. Shaw,† Irina Novozhilova,‖ Tao Liu,† Guy Jennings,‡ Klaus Attenkofer,‡ Gerald J. Meyer,*,§ and Philip Coppens*,‖

Contribution from Chemistry Division and Material Sciences Division, Argonne National Laboratory, Argonne, Illinois 60439, Department of Chemistry, Johns Hopkins University, Baltimore, Maryland 21210, and Department of Chemistry, State University of New York, Buffalo, New York 14260

Received November 25, 2002; E-mail: lchen@anl.gov

Abstract: The molecular structure and dynamics of the photoexcited metal-to-ligand-charge-transfer (MLCT) state of $[Cu^{I}(dmp)_2]^+$, where dmp is 2,9-dimethyl-1,10-phenanthroline, in acetonitrile have been investigated by time-domain pump-probe X-ray absorption spectroscopy, femtosecond optical transient spectroscopy, and density functional theory (DFT). The time resolution for the excited state structural determination was 100 ps, provided by single X-ray pulses from a third generation synchrotron source. The copper ion in the thermally equilibrated MLCT state has the same oxidation state as the corresponding copper(II) complex in the ground state and was found to be penta-coordinate with an average nearest neighbor Cu−N distance 0.04 Å shorter than that of the ground state $[Cu^{I}(dmp)_2]^+$. The results confirm the previously proposed "exciplex" structure of the MLCT state in Lewis basic solvents. The evolution from the photoexcited Franck-Condon MLCT state to the thermally equilibrated MLCT state was followed by femtosecond optical transient spectroscopy, revealing three time constants of 500−700 fs, 10−20 ps, and 1.6−1.7 ns, likely related to the kinetics for the formation of the triplet MLCT state, structural relaxation, and the MLCT excited-state decay to the ground state, respectively. DFT calculations are used to interpret the spectral shift on structural relaxation and to predict the geometries of the ground state, the tetracoordinate excited state, and the exciplex. The DFT calculations also indicate that the amount of charge transferred from copper to the dmp ligand upon photoexcitation is similar to the charge difference at the copper center between the ground-state copper(I) and copper(II) complexes.

Introduction

Photoexcited states of molecules are vehicles for solar energy conversion and storage, photosensitization, photocatalysis, and molecular devices.[1−5] However, structural information for excited state molecules has been sparse and indirect, in comparison with abundant and sophisticated kinetics information obtained by time-resolved optical spectroscopy. The recent development of time-domain X-ray structural techniques begins to enable molecular structure determination of highly energetic transient species with limited lifetimes in both crystalline and disordered forms, using similar pump−probe techniques employed in optical spectroscopy but with X-ray pulses as the probe.[6−17]

† Chemistry Division, Argonne National Laboratory.
‡ Material Sciences Division, Argonne National Laboratory.
§ Johns Hopkins University.
‖ State University of New York, Buffalo.

(1) Gust, D.; Moore, T. A.; Moore, A. L. *Acct. Chem. Res.* **2001**, *34*, 40−48.
(2) Balzani, V. *NATO ASI Ser., Ser. C* **1997**, *499*, 433−449.
(3) Fox, M. A. *Synthetic Applications of Photocatalytic Oxidation and Reduction Reactions of Organic Reactants on Irradiated Semiconductor Surfaces*; Wiley-VCH: New York, 2001; Vol. 1.
(4) Roundhill, D. M. *Photochemistry and Photophysics of Metal Complexes*; Plenum Press: New York, 1994.
(5) Mauch, R. H.; Gumlich, H. E. *Inorganic and Organic Electroluminescence*; Wissenschaft und Technik Verlag: Berlin, 1996.
(6) Kim, C. D.; Pillet, S.; Wu, G.; Fullagar, W. K.; Coppens, P. *Acta Crystl. A* **2002**, *58*, 133−137.
(7) Ozawa, Y.; Pressprich, M. R.; Coppens, P. *J. Appl. Crystallogr.* **1998**, *31*, 128−135.
(8) Tomov, I. V.; Oulianov, D. A.; Chen, P.; Rentzenpis, P. M. *J. Phys. Chem., B* **1999**, *103*, 7081−7091.
(9) DeCamp, M. F.; Reis, D. A.; Bucksbaum, P. H.; Adams, B.; Caraher, J. M.; Clarke, R.; Conover, C. W. S.; Dufresne, E. M.; Merlin, R.; Stoica, V.; Wahlstrand, J. K. *Nature* **2001**, *413*, 825−828.
(10) Larsson, J.; Chang, Z.; Judd, E.; Schuck, P. J.; Falcone, R. W.; Heimann, P. A.; Padmore, H. A.; Kapteyn, H. C.; Bucksbaum, P. H.; Murnane, M. M.; Lee, R. W.; Machacek, A.; Wark, J. S.; Liu, X.; Shan, B. *Opt. Lett.* **1997**, *22*, 1012−1014.
(11) Rose-Petruck, C.; Jimenez, R.; Guo, T.; Cavalleri, A.; Siders, C. W.; Raksi, F.; Squier, J. A.; Walker, B. C.; Wilson, K. R.; Barty, C. P. J. *Nature* **1999**, *398*, 310−312.
(12) Schoenlein, R. W.; Chattopadhyay, S.; Chong, H. H. W.; Glover, T. E.; Heimann, P. A.; Shank, C. V.; Zholents, A. A.; Zolotorev, M. S. *Science* **2000**, *287*, 2237−2240.
(13) Srajer, V.; Ren, Z.; Teng, T.-Y.; Schmidt, M.; Ursby, T.; Bourgeois, D.; Pradervand, C.; Schildkamp, W.; Wulff, M.; Moffat, K. *Biochemistry* **2001**, *40*, 13802−13815.
(14) Chen, L. X.; Jenings, G.; Liu, T.; Gosztola, D. J.; Hessler, J. P.; Scaltrito, D. V.; Meyer, G. J. *J. Am. Chem. Soc.* **2002**, *124*, 10861−10867.
(15) Chen, L. X.; Lee, P. L.; Gosztola, D.; Svec, W. A.; Montano, P. A.; Wasielewski, M. R. *J. Phys. Chem. B* **1999**, *103*, 3270−3274.
(16) Chen, L. X.; Jager, W. J. H.; Jennings, G.; Gosztola, D. J.; Munkholm, A.; Hessler, J. P. *Science* **2001**, *292*, 262−264.

10.1021/ja0294663 CCC: $25.00

Scheme 1

$$[Cu^{I}(dmp)_2]^{+} + h\nu \rightarrow [Cu^{II}(dmp^{-})(dmp)]^{+*}$$

The metal-to-ligand charge transfer (MLCT) excited states of cuprous diimine compounds are often luminescent and play important roles in photoinduced electron and energy transfer.[18−25] Meanwhile, these compounds are functional moieties in molecular devices because of their novel structural reorganization upon Cu^{I}/Cu^{II} interconversion, induced electrochemically or photochemically.[26,27] These reorganization processes are relevant to "gated" electron transfer in proteins[28,29] and model systems[18,30−33], as well as in solar energy conversion materials.[24,34] $[Cu^{I}(dmp)_2]^{+}$ (dmp = 2,9-dimethyl-1,10-phenanthroline) is one of the most extensively studied cuprous diimine compounds in which the origin of the photodriven structural change can be described by Scheme 1.

The Cu^{I} ground state has a d^{10} electronic configuration with pseudo-tetrahedral geometry.[35−40] The currently accepted mechanism for photogenerating the MLCT state is depicted in Figure 1. Absorption of a visible photon promotes an electron from the Cu^{I} center to one of the dmp ligands, generating a Franck−Condon (F−C) MLCT state with a Cu^{II}* center coordinated to one reduced and one neutral dmp ligand. The initial F−C MLCT state has the identical pseudo-tetrahedral coordination geometry as the ground state, but the Cu^{II}* center with a d^{9} electronic configuration is susceptible to a Jahn−Teller distortion resulting in an MLCT state with a flattened tetrahedral coordination, the flattened MLCT state. The large "Stokes-like" shift observed between the absorption and photoluminescence is consistent with significant structural changes in the flattened MLCT state that either returns to the ground state via a radiative decay pathway

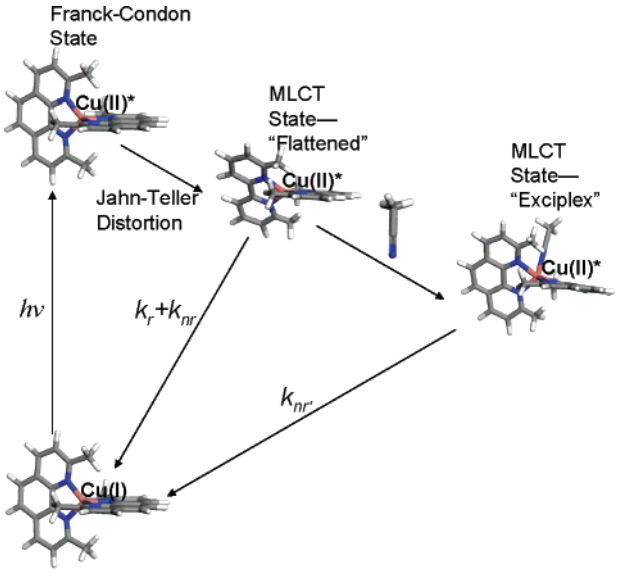

Figure 1. The mechanism of generation and decay of the MLCT state of $[Cu(dmp)_2]^{+}$ in acetonitrile depicted by literature.

or forms a pentacoordinate complex with strong Lewis basic solvents, resulting in the "exciplex" quenching in this ligated MLCT state.[41−51] Jahn−Teller effects were also seen in crystal structures of Cu^{II} bipyridine and phenanthroline compounds that display distorted square pyramidal or trigonal bi-pyramidal geometries with an additional ligand derived from a solvent molecule or counterion.[52−57] Nevertheless, the structural information on the MLCT state of $[Cu^{I}(dmp)_2]^{+}$, with or without the strong Lewis base, is mostly indirect so far, and the dynamics for the initial structural rearrangements have not been fully investigated.

Recently, the structure of an MLCT state of $[Cu^{I}(dmp)_2]$BArF (BArF = tetrakis(3,5-bis(trifluoromethylphenyl)borate)) in presumed noncoordinating toluene was characterized using laser pulse pump, X-ray pulse probe X-ray absorption spectroscopy (XAS).[14] In this specific study, a laser pulse created an F−C MLCT state of $[Cu^{I}(dmp)_2]^{+}$ with a Cu^{II}* center in the ground-

(17) Neutze, R.; Wouts, R.; Techert, S.; Davidsson, J.; Kocsis, M.; Kirrander, A.; Schotte, F.; Wulff, M.; *Phys. Rev. Lett.* **2001**, *87*, 195508/1−195508/4.
(18) Ahn, B.-T.; McMillin, D. R. *Inorg. Chem.* **1981**, *20*, 1427−1432.
(19) Blasse, G.; McMillin, D. R. *Chem. Phys. Lett.* **1980**, *70*, 1−3.
(20) Buckner, M. T.; McMillin, D. R. *J. Chem. Soc., Chem. Commun.* **1978**, 759−761.
(21) Dietrich-Buchecker, C. O.; Marnot, P. A.; Sauvage, J. P.; Kirchoff, J. R.; McMillin, D. R. *J. Chem. Soc., Chem. Commun.* **1983**, 513−515.
(22) Castellano, F. N.; Ruthkosky, M.; Meyer, G. J. *Inorg. Chem.* **1995**, *34*, 3−4.
(23) Miller, M. T.; Ganzel, P. K.; Karpishin, T. B. *Angew. Chem., Int. Ed.* **1998**, *37*, 1556.
(24) Ruthkosky, M.; Kelly, C. A.; Zaros, M. C.; Meyer, G. J. *J. Am. Chem. Soc.* **1997**, *119*, 12004−12005.
(25) Miller, M. T.; Ganzel, P. K.; Karpishin, T. B. *J. Am. Chem. Soc.* **1999**, *121*, 4292.
(26) Collin, J.-P.; Dietrich-Buchecker, C.; Gavina, P.; Jimenez-Molero, M. C.; Sauvage, J.-P. *Acc. Chem. Res.* **2001**, *34*, 477−487.
(27) Kern, J.-M.; Raehm, L.; Sauvage, J.-P.; Divisia-Blohorn, B.; Vidal, P.-L. *Inorg. Chem.* **2000**, *39*, 1555−1560.
(28) Fox, S.; Nanthakumar, A.; Wikstrom, M.; Karlin, K. D.; Blackburn, N. J. *J. Am. Chem. Soc.* **1996**, *118*, 24−34.
(29) Kleinfeld, D.; Okamura, M. Y.; Feher, G. *Biochim. Biophys. Acta* **1984**, *766*, 126−140.
(30) Cunningham, K. L.; McMillin, D. R. *Inorg. Chem.* **1998**, *37*, 4114−4119.
(31) Meagher, N. E.; Juntunen, K. L.; Salhi, C. A.; Ochrymowycz, L. A.; Rorabacher, D. B. *J. Am. Chem. Soc.* **1992**, *114*, 10411−10420.
(32) Flanagan, S.; Dong, J.; Haller, K.; Wang, S.; Scheidt, W. R.; Scott, R. A.; Webb, T. R.; Stanbury, D. M.; Wilson, L. J. *J. Am. Chem. Soc.* **1997**, *119*, 8857−8864.
(33) Koshino, N.; Kuchiyama, Y.; Ozaki, H.; Funahashi, S.; Takagi, H. D. *Inorg. Chem.* **1999**, *38*, 3352−2260.
(34) Alonso-Vante, N.; Nierengarten, J. F.; Sauvage, J. P. *J. Chem. Soc., Dalton Trans.* **1994**, 1649.
(35) Stephens, F. S.; Tucker, P. A. *J. Chem. Soc., Dalton Trans.* **1973**, 2293.
(36) Kaiser, J.; Bauer, G.; Schroder, F. A.; Taylor, I. F.; Rasmussen, S. E. *J. Chem. Soc., Dalton Trans.* **1974**, 1490.
(37) Anderson, O. P. *Inorg. Chem.* **1975**, *14*, 730.
(38) Harrison, W. D.; Hathaway, B. J.; Kennedy, D. A. *Acta Crystl. Sect. B* **1979**, *35*, 2301.
(39) Tran, D.; Skelton, B. W.; White, A. H.; Laverman, L. E.; Ford, P. C. *Inorg. Chem.* **1998**, *37*, 2505−2511.
(40) Shinozaki, K.; Kaizu, Y. *Bull. Chem. Soc. Jpn.* **1994**, *67*, 2435−2439.
(41) Kalyanasundaram, K. *Photochemistry of Polypyridine and Porphyrin Complexes*; Academic Press: London, 1992.
(42) Cunningham, C. T.; Cunningham, K. L. H.; Michalec, J. F.; McMillin, D. R. *Inorg. Chem.* **1999**, *38*, 4388−4392.
(43) Everly, R. M.; McMillin, D. R. *Photochem. Photobiol.* **1989**, *50*, 711−716.
(44) Hudson, B. P.; Sou, J.; Berger, D. J.; McMillin, D. R. *J. Am. Chem. Soc.* **1992**, *114*, 8997−9002.
(45) Ichinaga, A. K.; Kirchhoff, J. R.; McMillin, D. R.; Dietrich-Buchecker, C. O.; Marnot, P. A.; Sauvage, J. P. *Inorg. Chem.* **1987**, *26*, 4290−4292.
(46) McMillin, D. R.; Kirchhoff, J. R.; Goodwin, K. V. *Coord. Chem. Rev.* **1985**, *64*, 83−92.
(47) Palmer, C. E. A.; McMillin, D. R. *Inorg. Chem.* **1987**, *26*, 3837−3840.
(48) Palmer, C. E. A.; McMillin, D. R.; Kirmaier, C.; Holten, D. *Inorg. Chem.* **1987**, *26*, 3167−3170.
(49) Scaltrito, D. V.; Thompson, D. W.; O'Callaghan, J. A.; Meyer, G. J. *Coord. Chem. Rev.* **2000**, *208*, 243−266.
(50) Stacy, E. M.; McMillin, D. R. *Inorg. Chem.* **1990**, *29*, 393−396.
(51) Tamilarasan, R.; McMillin, D. R. *Inorg. Chem.* **1990**, *29*, 2798−2802.
(52) Cunningham, C. T.; Moore, J. J.; Cunningham, K. L. H.; Fanwick, P. E.; McMillin, D. R. *Inorg. Chem.* **2000**, *39*, 3638−3644.
(53) Burke, P. J.; Henrick, K.; McMillin, D. R. *Inorg. Chem.* **1982**, *21*, 1881−1886.
(54) Kirchhoff, J. R.; McMillin, D. R.; Robinson, W. R.; Powell, D. R.; McKenzie, A. T.; Chen, S. *Inorg. Chem.* **1985**, *24*, 3928−3933.
(55) Klemens, F. K.; Palmer, C. E. A.; Rolland, S. M.; Fanwick, P. E.; McMillin, D. R.; Sauvage, J. P. *New J. Chem.* **1990**, *14*, 129−133.
(56) Schatz, M.; Becker, M.; Thaler, F.; Hampel, F.; Schindler, S.; Jacobson, R. R.; Tyeklar, Z.; Murthy, N. N.; Ghosh, P.; Chen, Q.; Zubieta, J.; Karlin, K. D. *Inorg. Chem.* **2001**, *40*, 2312−2322.
(57) Van Meerssche, M.; Germain, G.; Declercq, J. P. *Crystal Struct. Commun.* **1981**, *10*, 47−53.

state geometry. Within the time resolution of the experiment (i.e., 14 ns), this state rapidly underwent vibrational relaxation and Jahn−Teller distortion to yield an emissive MLCT state that lived for about 100 ns. The results of the experiment demonstrated that (1) light excitation generated a formally Cu^{II}* center, (2) the inner-sphere reorganization changed the coordination number of the MLCT state from four to five in presumed noncoordinating toluene, and (3) the average Cu-ligand bond distances lengthened in the MLCT state. On the basis of these observations and the emissive nature of the MLCT state, we suggested that light absorption and emission involved two distinct geometries and at least four states were involved in the photophysics.[14]

In the present study, a strong Lewis base, acetonitrile, is used as the solvent that may ligate with the formally Cu^{II}* in the MLCT state of $[Cu^{I}(dmp)_2]^+$ to form an exciplex.[33,42,48,58−60] Unlike the MLCT state of $[Cu^{I}(dmp)_2]^+$ in toluene, the absence of room-temperature luminescence and a much shorter lifetime of 2 ns for the MLCT state of $[Cu^{I}(dmp)_2]^+$ in acetonitrile were interpreted as strong evidence for the exciplex quenching, due to the ligation of acetonitrile with the Cu^{II}* center.[48] In this study, single X-ray pulses with 100-ps fwhm were used to probe the structure of the MLCT state of $[Cu^{I}(dmp)_2]^+$ in acetonitrile by the pump−probe XAS. Hence, the intrinsic time resolution in this study is over 2 orders of magnitude better than in the previous study. Although the pulse duration of a single X-ray pulse from the synchrotron source is adequate for probing the structure of the flattened or ligated MLCT state, it is still too long for following atomic evolution from the F−C MLCT state to these longer-lived MLCT states. At present, we investigate the dynamics of this fast process through femtosecond (fs) optical transient spectroscopy, leaving the fast atomic movements to be followed by ultrafast X-ray pulses with sufficient photon flux in the future.[9−12,61−63] The flattened and ligated MLCT state structures as well as the molecular orbitals involved in the photoexcitation of $[Cu^{I}(dmp)_2]^+$ were calculated by the DFT in the absence and the presence of HCN as the fifth ligand as a model for acetonitrile. With the combined information on the MLCT state structures, the energy levels of the molecular orbitals, and the excited-state dynamics, we can gain insight into structural factors governing the excited-state properties that make $[Cu^{I}(dmp)_2]^+$ an attractive choice for energy and electron-transfer processes in various potential applications.

Experimental Methods

Pump−Probe XAS. The laser pulse pump, X-ray pulse probe time-domain XAS at the copper K-edge (8.979 keV) experiments, including X-ray absorption near edge structure (XANES) and X-ray absorption fine structure (XAFS) measurements, were conducted at a wiggler beamline, 11ID-D, Basic Energy Science Synchrotron Research Center of the Advanced Photon Source at Argonne National Laboratory. Details of the experimental setup have been described elsewhere.[14,16,64,65] A monochromator with Si 220 crystals provided an energy resolution of 0.5 eV at 9 keV. The pump laser pulses were from the second harmonic output of a Nd/YLF laser (λ = 527 nm, 1 kHz repetition rate, 1mJ/pulse and 5 ps fwhm). The probe X-ray pulses with fwhm of ~ 100 ps were generated from single electron bunches, each of which was separated in time from other pulses in the storage ring.[14,16,64,65] The time delay between the pump and the probe was adjusted so that the laser pulse preceded the X-ray pulse by less than 200 ps. The laser pump and X-ray probe beams were overlapped at a continuously flowing stream of 2 mM $[Cu^{I}(dmp)_2](PF_6)$ acetonitrile solution, with about 0.5 mm thickness. Argon gas was bubbled through the solution reservoir to minimize radiation damage of the sample. The XAFS spectra were collected in the fluorescence mode using a multielement Ge detector array (Canberra). Because the repetition rate of the laser (1 kHz) was much lower than the X-ray pulses (271 kHz) and only 5 mA of the total 100 mA storage ring current was allocated to provide the isolated single X-ray pulse, only ~0.02% of the total X-ray photon flux was used to probe the MLCT state structure. To extract the X-ray fluorescent signals with and without the laser, signals from the Ge detector array were split into two equal parts and connected separately to two scalar modules. The first module processed X-ray signals from probe pulses, and its output was used to obtain the spectra of the laser-excited sample. The second module processed signals from all X-ray pulses, and its output was used to construct the spectra of the ground state, neglecting the 0.02% contribution from the laser-excited sample. The pump−probe cycles were repeated at the laser pulse repetition rate of 1 kHz until the XAFS spectrum of the laser excited sample had a sufficient signal-to-noise ratio to establish the oxidation state, the coordination geometry, and local fine structure around the metal center. The total data acquisition time was approximately 40 h, during which the sample solution was replaced every few hours to ensure the integrity of the sample. UV−Vis spectra of the sample solution taken after the experiment showed no significant change from the starting solution. Thus, the integrity of the sample solution was maintained during the measurements.

Data Analysis of XANES and XAFS Spectra. For the XAFS data analysis, the $[Cu^{I}(dmp)_2](NO_3)$ crystal structure[66] was used as reference for the ground-state structure in solution (the coordination number = 4, the average Cu−N distance = 2.07 Å), assuming that the solid and the solution structures were the same. WinXAS 97 (T. Ressler) was used for data analysis following standard procedures. The experimentally collected data after the Fourier back transform was fit to the equation

$$\chi(\mathrm{k}) = \Sigma \mathrm{F}_i(k)\mathrm{S}_0{}^2(k)\mathrm{N}_i/(k\mathrm{R}_i{}^2) \cdot \exp(-2\sigma_i{}^2k^2)\sin[2k\mathrm{R}_\mathrm{i} + \phi_\mathrm{i}(k)] \quad (1)$$

where F(k) is the magnitude of the backscattering; S_0, amplitude reduction factor; N, the coordination number; R, the average distance; σ^2, the Debye−Waller factor; and ϕ_i, the phase shift; the subscript indicates i-th atom; and k is the electron wavevector.

Because photoexcitation rarely converts all molecules to the excited state, the X-ray absorption of the laser pumped sample is from a mixture of the ground and the excited states, as described below

$$\mu(E,t) = [1 - \sum_j f_{esj}(t)]\mu_{gs}(E) + \sum_j f_{esj}(t)\mu_{esj}(E,t) \quad (2)$$

where $\mu(E,t)$ is the total absorption at X-ray photon energy E and time t, $f_{esj}(t)$ is the fraction of the j-th excited state at t, and the subscripts gs and es stand for the ground and excited states, respectively. $\mu_{esj}(E,t)$ accounts for the atomic movements as a function of t, and $f_{esj}(t)$, for the population decay in the same excited state with t. When the time resolution of the experiment is approximately 100 ps from a synchrotron

(58) Blaskie, M. W.; McMillin, D. R. *Inorg. Chem.* **1980**, *19*, 3519−3522.
(59) Crane, D. R.; DiBenedetto, J.; Palmer, C. E. A.; McMillin, D. R.; Ford, P. C. *Inorg. Chem.* **1988**, *27*, 3698−3700.
(60) McMillin, D. R.; Drago, R. S.; Nusz, J. A. *J. Am. Chem. Soc.* **1976**, *98*, 3120−3126.
(61) Chin, A. H.; Schoenlein, R. W.; Glover, T. E.; Balling, P.; Leemans, W. P.; Shank, C. V. *Phys. Rev. Lett.*, **1999**, *83*, 336−339.
(62) Anderson, T.; Tomov, I. V.; Rentzepis, P. M. *J. Chem. Phys.*, **1993,** *99*, 869−875.
(63) Murnane, M. M.; Kapteyn, H. C.; Falcone, R. W. *IEEE J. Quantum Electron.* **1989**, *25*, 2417−2422.
(64) Chen, L. X. *J. Electron Spectrosc. Relat. Phenom.* **2001**, *119*, 161−174.
(65) Jennings, G.; Jaeger, W. J. H.; Chen, L. X. *Rev. Sci. Inst.* **2002**, *72*, 362−368.
(66) Hamalainen, R.; Algren, M.; Turpeinen, U.; Raikas, T. *Crystal Struct. Commun.* **1979**, *8*, 75−80.

source, $\mu_{esj}(E,t)$ can be viewed as static, $\mu_{esj}(E)$. Therefore, eq 2 can be approximated as

$$\mu(E,t) = [1 - \sum_j f_{esj}(0)e^{-k_j t}]\mu_{gs}(E) + \sum_j f_{esj}(0)e^{-k_j t}\mu_{esj}(E) \quad (3)$$

where $f_{esj}(0)$ is the initial fraction of the j-th excited state, and k_j is the time constant for the j-th excited state population decay, assuming the first order process. Further simplification can be made if only one thermally equilibrated excited state dominates. In this case, the time delay between the laser pump and the X-ray probe pulses is set to probe the excited state structure at its optimal concentration, normally at time "zero", which is within 100 ps after the pump laser pulse in our experiments. Equation 3 can be simplified as

$$\mu(E) = [1 - f_{es}(0)]\mu_{gs}(E) + f_{es}(0)\mu_{es}(E) \quad (4)$$

In general, $\mu_{es}(E)$ and $f_{es}(0)$ are both unknown, which imposes two unknowns in eq 4. $f_{es}(0)$ can be obtained by pump−probe optical transient spectroscopic measurements conducted simultaneously conducted with the pump−probe XAFS or separately with the same conditions for the photoexcitation. $\mu_{es}(E)$ can be estimated sometimes when a priori knowledge of the excited structure is available, especially in the XANES region. More frequently, $f_{es}(0)$ value can be calculated from the Beer−Lambert law for light absorption, $I_t = I_o \cdot 10^{-\epsilon lC}$, where I_t and I_o are transmitted and incident laser light intensities, respectively, ϵ is the molar extinction coefficient (M^{-1} cm^{-1}), l and C are the length of the light path (cm), and the concentration of the ground-state molecules in the sample (M). Light intensity absorbed by the sample is I_o ($1-10^{-\epsilon lC}$). Assuming that the laser pulse energy is P_o (in J), the number of absorbed photons from each pump laser pulse is $N_a = P_o/h\nu \cdot (1-10^{-\epsilon lC})$, where N_a is the number of photons absorbed by the sample from each pump pulse, and $h\nu$ is the energy per quanta of the laser photon. $f_{es}(0)$ can be obtained by solving the equation

$$f_{es}(0) = \frac{P_0 \cdot Q\{1 - 10^{-\epsilon \cdot l \cdot C_{total}[1-f_{es}(0)]}\}}{h\nu \cdot C_{total} \cdot a \cdot l \cdot A} \quad (5)$$

where a is the laser pump pulse illuminated area at the sample, A is the Avogadro constant, and Q is the quantum yield for generating the excited state. Equation 5 addresses the relationships between $f_{es}(0)$ and experimental parameters, such as laser beam size, sample thickness, molar distinction coefficient, total concentration of the sample, and the pump pulse energy. Equation 5 is also based on the assumption that the excited-state absorption at the excitation wavelength can be neglected. With the guidance of eq 5, $f_{es}(0)$ can be estimated for a particular experimental condition and used in solving eq 4.

For the laser-excited sample, the nearest neighbor distances were fit to both one- and two-distance models, and the goodness of the fit was judged by the fitting residuals. If the residuals were reduced by more than a factor of 2 in the two-distance model compared to the one-distance model, the results were considered plausible. The ground-state structural parameters served as the references for fitting the MLCT structure with the two-distance model, where the relative fraction and the distance for the remaining ground state were fixed during in the fitting. We found that this method was superior to using the structural parameters from a Cu^{II} complex (as we did before) in terms of finding the structural differences between the ground and the MLCT state, because the spectra of the reference (the ground state) and the unknown (the MLCT state) were taken at the same time and under the same experimental conditions.

Ultrafast Optical Transient Absorption. Transient absorption measurements were performed with an apparatus based on an amplified Ti/sapphire laser system as described elsewhere.[67] The 417 nm excitation pulses were obtained from the second harmonic of the output from the Ti:Sapphire amplifier. White light continuum probe pulses were generated by focusing a few μJ of the Ti/sapphire amplifier output onto a sapphire disk. The white light was split into two beams that served as the reference and the probe, respectively. The probe beam and the 300 nJ pump beam were focused to a 0.3 mm spot size at the sample in a nearly collinear geometry. The sample cuvette's path length was 2 mm. The widths of the pump and probe pulses were about 100 fs, and the total instrumental response for the pump−probe experiments was about 180 fs. The transient absorption changes at a particular probe wavelength as a function of time was analyzed by fitting the data with using a multiexponential kinetic model convoluted with convolution of a Gaussian instrument response function with 180 fs fwhm.

Samples. The $[Cu^I(dmp)_2](PF_6)$ was synthesized according to previously published procedures.[46,58] The acetonitrile was from Aldrich. The sample solution with a concentration of 2 mM was used in the XAFS measurement. The solution sample used in the transient optical absorption measurements was about 0.4 mM and was used without degassing.

Computational Methods. Calculations were carried out with the ADF2002.01 suite of programs.[68−70] The calculations made use of the local density approximation (LDA) functional of Vosko-Wilk-Nusair (VWN)[71], plus the generalized gradient approximation (GGA) with the exchange functional of Becke and the correlation functional of Lee−Yang−Parr (B88LYP). The atomic orbitals of copper were described by a triple-ζ Slater-type basis set (ADF database TZP, former IV). The carbon, nitrogen, and hydrogen atoms were described by double-ζ Slater-type basis sets with one polarization function added on C, N, and H (ADF database DZP, former III). The $(1s2s2p)^{10}$ core shell of Cu and $(1s)^2$ core shell of C and N were treated by the frozen-core approximation. Relativistic effects were taken into account using the zeroth order regular approximation (ZORA).[72−75] The integrals were evaluated numerically with an accuracy of 8 significant digits. A set of auxiliary s, p, d, f, and g functions, centered on all nuclei, was used to fit the electron density as well as both Coulomb and exchange potentials in each self-consistent field (SCF) cycle. The D_2 point group was used to optimize the ground state, while *no symmetry restrictions* were applied to the excited state. The triplet excited state was chosen to model the thermally equilibrated MLCT state, because the intersystem crossing is very fast and efficient (see below). The ground state was converged to the threshold of 10^{-4} Hartree/Å on the Cartesian gradients. Convergence of the excited state was very difficult to attain with this strict threshold. In the interest of time, the geometry convergence of the excited state was set to the threshold of 10^{-3} Hartree/Å on the Cartesian gradients. With this convergence criteria, the energy difference between the last two optimization cycles for the excited state was of the order 10^{-4} Hartree, (~0.06 kcal/mol), which is the same as that reported in DFT study of Co_3(dipyridylamide)$_4Cl_2$ complex.[76a] All optimized molecular geometries were confirmed as true energy minima by observation of only positive eigenvalues in the Hessian matrixes. The molecular orbitals were visualized with MOLDEN3.7.[77] The ADF output data were converted to MOLDEN format using ADF2MOLDEN

(67) Greenfield, S. R.; Svec, W. A.; Gosztola, D. J.; Wasielewski, M. R. *J. Am. Chem. Soc.* **1996**, *118*, 6767.
(68) te Velde, G.; Bickelhaupt, F. M.; van Gisbergen, S. J. A.; Fonseca Guerra, C.; Baerends, E. J.; Snijders, J. G.; Ziegler, T. *J. Comput. Chem.* **2001**, *22*, 931−967.
(69) Fonseca Guerra, C.; Snijders, J. G.; te Velde, G.; Baerends, E. J. *Theor. Chem. Acc.* **1998**, *99*, 391−403.
(70) ADF2002.01, S., Theoretical Chemistry, Vrije Universiteit, Amsterdam, The Netherlands, http://www.scm.com.
(71) Vosko, S. H.; Wilk, L.; Nusair, M. *Can. J. Phys.* **1980**, *58*, 1200−1211.
(72) Chang, C. H.; Pelissier, M.; Durand, M. *Phys. Scr.* **1986**, *34*, 394−404.
(73) van Lenthe, E.; Baerends, E. J.; Snijders, J. G. *J. Chem. Phys.* **1993**, *99*, 4597−4610.
(74) van Lenthe, E.; Baerends, E. J.; Snijders, J. G. *J. Chem. Phys.* **1994**, *101*, 9783−9792.
(75) van Lenthe, E.; van Leeuwen, R.; Baerends, E. J.; Snijders, J. G. *Int. J. Quantum Chem.* **1996**, *57*, 281−293.
(76) (a) Rohmer, M.-M.; Strich, A.; Benard, M.; Malrieu, J.-P. *J. Am. Chem. Soc.* **2001**, *123*, 9126−9134. (b) Ricciardi, G.; Rosa, A.; Baerends, E. J.; van Gisbergen, S. A. J. *J. Am. Chem. Soc.* **2002**, *124*, 12319−12334.
(77) Schaftenaar, G.; Noordik, J. H. *J. Comput.-Aided Mol. Design* **2000**, *14*, 123−134.

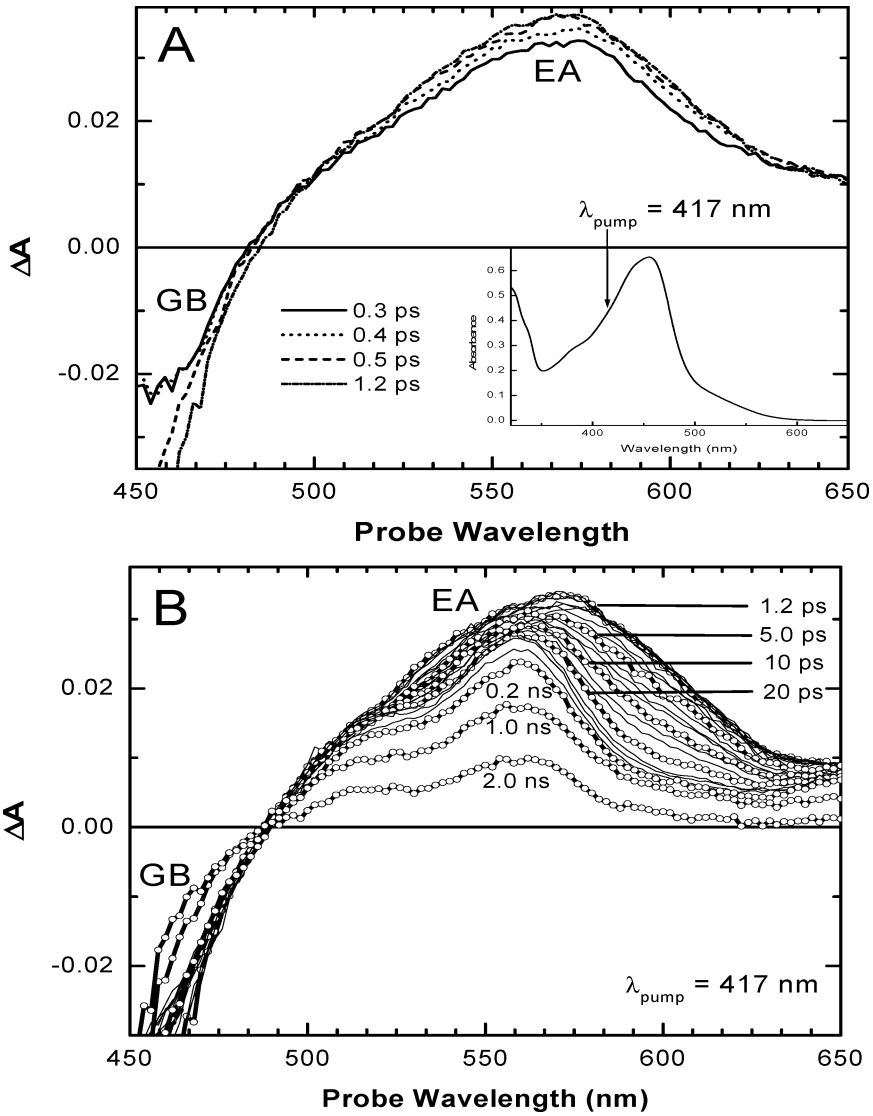

Figure 2. The transient absorption of $[Cu^{I}(dmp)_2]^+$ in acetonitrile (A) within 1.2 ps after the excitation along with the ground-state absorption (inset) and (B) from 1.2 ps to 2 ns.

program.[78] Time-dependent density functional theory (TD-DFT)[79−81] calculations were carried out with the same functional used in the geometry optimization. The TD-DFT calculations were performed for the ground-state D_2 geometry at different values of the dihedral angle between the dmp planes. The Davidson algorithm was used, in which the error tolerance in the square of the excitation energies and trial-vector orthonormality criterion were set to 10^{-8} and 10^{-10}, respectively.

Results

Photoexcitation Dynamics of the MLCT State of $[Cu(I)(dmp)_2]^+$ in Acetonitrile. Transient absorption spectra of $[Cu^{I}(dmp)_2]^+$ in acetonitrile excited by 417 nm light are shown in Figure 2, where the spectra within the first 1.2 ps after the photoexcitation are displayed separately along with the ground state absorption (Figure 2A). The negative change in the absorbance in the region from 450 up to 480 nm is dominated by the ground-state bleaching (GB), while the positive change in the absorbance in the region above 480 nm is mainly due to the excited-state absorption (EA). There is an apparent rise of the entire absorption band between 480 and 620 nm within the first 1.2 ps without the fine features that appeared later. In the same spectral region, the well-documented double-peak feature, assigned to the $dmp^{\bullet -}$ absorption,[48,82] developed about 10−20 ps later, as results of a blue-shift and spectral narrowing from the red-side of the absorption peak from 570 to 600 nm (Figure 2B), followed by the decay of the entire absorption band with a time constant of about 1.6−1.7 ns. As a first approximation, kinetics at different wavelengths were fit to a sum of exponential functions, $f(t) = \Sigma A_i \exp(-t/\tau_i)$, assuming that only first-order processes were involved. Most of the kinetics traces require triexponential fits, with time constants $\tau = 1.5-1.7$ ns, 10−20 ps, and 0.2−0.8 ps (Table 1).

The absorbance changes measured at different wavelengths during first 40 ps after the laser pump pulse are depicted in Figure 3. At 475 nm, the transient absorption was due to GB, best described by a 0.5 ps rise of the bleaching, a 12 ps fast recovery, and the 1.6 ns slower recovery. The 1.6 ns time

(78) Volkov, A. V. State University of New York at Buffalo, 1999.
(79) van Gisbergen, S.; Kootstra, F.; Schipper, P. R. T.; Gritsenko, O. V.; Snijders, J. G.; Baerends, E. *Phys. Rev. A* **1998**, *57*, 2556−2571.
(80) Jamorski, C.; Casida, M. E.; Salahub, D. R. *J. Chem. Phys.* **1996**, *104*, 5134−5147.
(81) Bauernschmitt, R.; Ahlrichs, R. *Chem. Phys. Lett.* **1996**, *256*, 454−464.
(82) Gordon, K. C.; McGarvey, J. J. *Inorg. Chem.* **1991**, *30*, 2986−2989.

Table 1. Excited State Kinetic Parameters of $[Cu^{I}(dmp)_2]^{+}$ in Acetonitrile

params	475 nm	500 nm	520 nm	540 nm	560 nm	580 nm	600 nm
A_1[a]	0.015	0.008	0.004	−0.004	−0.032	−0.036	−0.011
τ_1 (ps)[b]	0.48 ± 0.03	0.52 ± 0.05	0.50 ± 0.15	0.19 ± 0.05	0.22 ± 0.01	0.27 ± 0.007	0.76 ± 0.03
A_2[a]	−0.007	−0.005	−0.008		−0.002	0.007	0.011
τ_2 (ps)[b]	12.0 ± 0.4	17.0 ± 0.5	15.4 ± 0.4		21.4 ± 1.9	12.7 ± 0.3	9.7 ± 0.1
A_3[a]	−0.020	0.007	0.020	0.017	0.023	0.019	0.008
τ_3 (ps)[b]	1645 ± 11	1742 ± 22	1696 ± 11	1671 ± 12	1615 ± 9	1750 ± 11	1515 ± 14

[a] The coefficients of the exponentials used in the fits $f(t) = \Sigma A_i \exp(-t/\tau_i)$, where positive values are the coefficients for the decay of the transient absorption and negative values are the coefficients for the recovery or the rise of the transient absorption. [b] The errors in time constants reflect the residual distribution in the fitting for the particular kinetics trace.

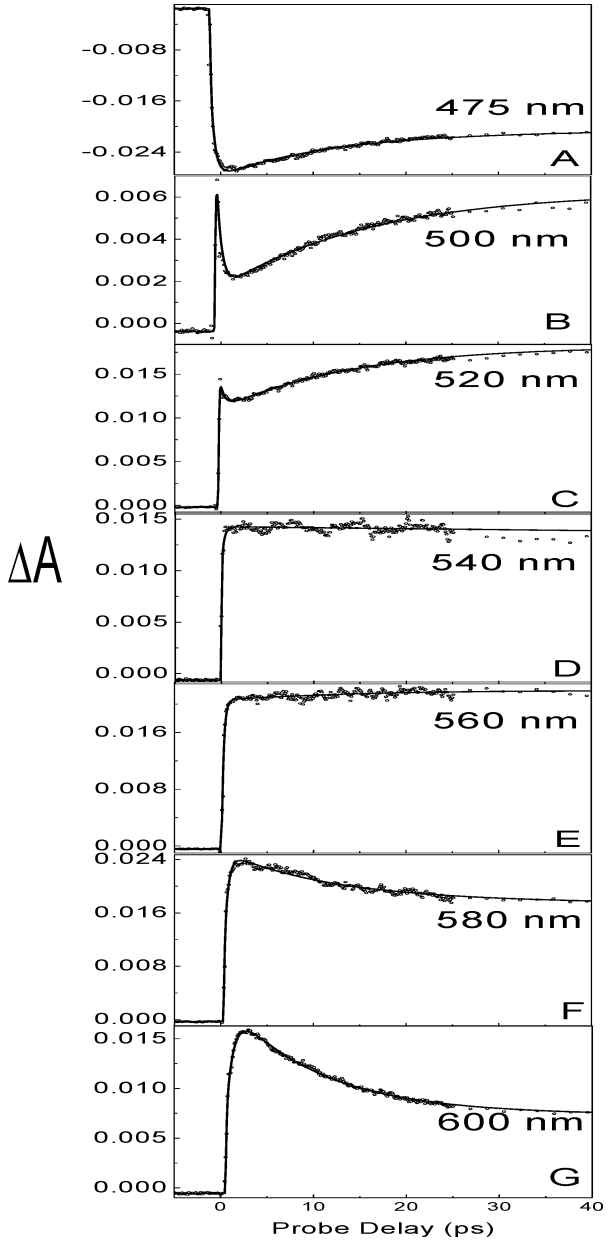

Figure 3. Transient absorption kinetics probed at different wavelengths within 40 ps after the photoexcitation of $[Cu^{I}(dmp)_2]^{+}$ in acetonitrile. The excitation wavelength is 417 nm and the probe wavelengths are as labeled.

constant for the ground-state recovery agrees with the MLCT state lifetime measured earlier with longer laser pulses.[48] However, the faster time constants of 12 and 0.5 ps were not reported before. In the region of 500−520 nm, where the ground state $[Cu^{I}(dmp)_2]^{+}$ has absorption coefficients ranging between 1000 and 2000 M^{-1} cm^{-1}, the kinetics traces are the superposition of both the ground-state recovery and the excited-state decay (Figure 3, parts B and C) resulting in the sharp feature near time zero. In the region of 540−560 nm, the absorption from the ground state became nearly negligible; hence, the contribution from GB was no longer observed. The initial rise time at both wavelengths was around 200 fs, followed by a 1.6 ns decay, but an additional 21 ps rise component is required to fit the transient absorption measured at 560 nm. At wavelengths longer than 560 nm, a blue shift was responsible for the spectral narrowing in the EA. The observed EA decays at both 580 and 600 nm have a sub-ps rise and double exponential decay components. The decay time constants of 1.75 and 1.51 ns at the two wavelengths, respectively, were comparable to the slow components observed at other wavelengths and in agreement with previous results.[48] However, the rise time of 760 fs at 600 nm was comparable to the bleaching time of 500 fs for the ground state. In addition, the 13 and 10 ps decay components at 580 and 600 nm had an apparent correspondence with the 12 ps component observed in GB at 475 nm. The origins of the sub-ps and 12-ps components in both blue and red sides of the transient absorption band require further discussion.

The MLCT State Structure from Time-Domain XAFS. According to the optical transient absorption results presented above, the longest time constant in the MLCT state decay kinetics was 1.6 ns in acetonitrile at room temperature (Figure 4), corresponding to the lifetime of the ligated MLCT state. Therefore, single X-ray pulses from the synchrotron with 100-ps fwhm provide sufficient time resolution for probing the structure of this MLCT state. Differences between the X-ray absorption near edge structure (XANES) spectra of the ground state and the laser excited $[Cu^{I}(dmp)_2]PF_6$ in acetonitrile are clearly visible in Figure 5. Similar to the previous study on $[Cu^{I}(dmp)_2]BArF$ in toluene,[14] the shoulder feature at 8.985 keV was reduced upon laser excitation, accompanied by a slight increase of the peak intensity at 8.996 keV.

To extract the spectrum for the MLCT state of $[Cu^{I}(dmp)_2]PF_6$, the XANES spectrum from the remaining ground state $[Cu^{I}(dmp)_2]PF_6$ must be subtracted from the spectrum of the laser excited sample where both states were present. On the basis of our previous calculations with eq 5 and measurements with the same experimental conditions,[14] about 20% of the ground state $[Cu^{I}(dmp)_2]PF_6$ would be converted to the MLCT state. Hence, the XANES spectrum for the MLCT state of $[Cu^{I}(dmp)_2]PF_6$ in acetonitrile shown in Figure 5B was obtained after subtracting the ground-state contributions. As in the previous study on $[Cu^{I}(dmp)_2]BArF$ in toluene,[14] the shoulder feature for the ground state $[Cu^{I}(dmp)_2]PF_6$ is missing in the MLCT state, and the transition edge is shifted by about 3 eV to the same edge energy as the ground state $[Cu^{II}(dmp)_2]^{2+}$ (Figure

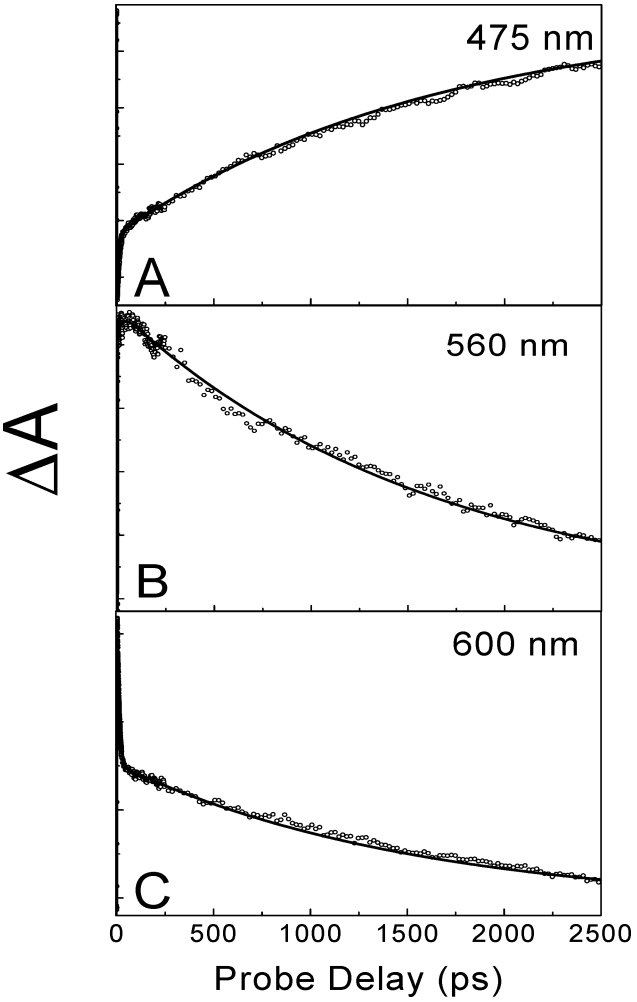

Figure 4. Transient absorption kinetics of $[Cu^{I}(dmp)_2]^+$ in acetonitrile excited by 417 nm light and probed at (A) 475 nm, (B) 560 nm, and (C) 600 nm. The transient absorption signal returns to the baseline at longer times (not shown).

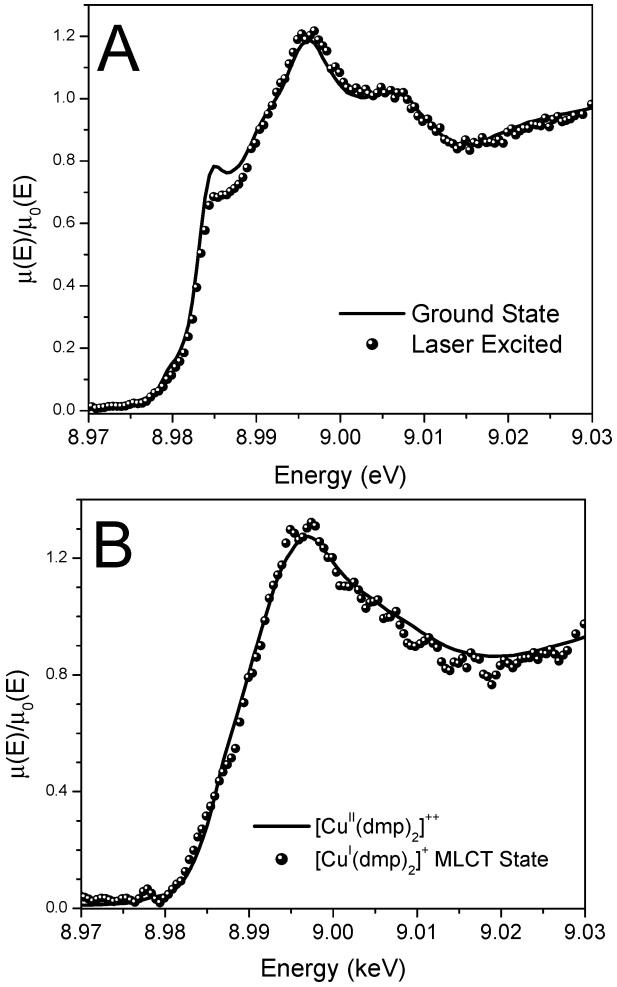

Figure 5. (A) The XANES spectra of the ground state and the laser excited $[Cu^{I}(dmp)_2]^+$ in acetonitrile. The spectrum of the laser-excited sample is an algebraic sum of the spectra for the ground state and the MLCT state. The estimated fraction for the excited state is about 20%. (B) The XANES spectrum of the MLCT state of $[Cu^{I}(dmp)_2]^+$ obtained from the difference spectrum between the laser-excited sample and the 80% ground-state spectrum normalized to the same edge jump level, along with the ground-state XANES spectrum of $[Cu^{II}(dmp)_2]^{2+}$ in acetonitrile, generated electrochemically.

5B). The shoulder feature at 8.985 keV is pronounced in $[Cu^{I}(dmp)_2]^+$ and missing from $[Cu^{II}(dmp)_2]^{2+}$. This shoulder feature originates from the 1*s* to 4p_z transition and reflects the nature of the 4p_z in different coordination environments.[83,84] When the first row transition metal is tetracoordinated, the 4p_z is virtually empty and localized, giving rise to a sharp 1*s* to 4p_z transition peak, as seen in the ground state of $[Cu^{I}(dmp)_2]^+$. However, when the transition metal is penta- or hexa-coordinated, the 4p_z orbital delocalizes over the ligands, resulting in a broad and smooth 1*s* to 4p_z transition feature.[83,84] Thus, the changes observed in Figure 5B are typical for transformation from 4- to 5- or 6-coordinate geometry.[83,84] The transition edge position for the MLCT state coincides with that of the Cu^{II} species and reflects a higher ionization energy required for ejecting the 1s electron from an ion with a more positive charge. The peak intensity at 8.997 keV in Figure 5A is higher for the laser-excited sample than that of the ground state, suggesting a higher average coordination number in the former, because of the proportionality of the oscillation amplitude with the coordination number in a particular neighboring shell.

The copper coordination number and the Cu-to-ligand bond lengths for the MLCT state of $[Cu^{I}(dmp)_2]^+$ were extracted from the XAFS data. Figure 6 displays XAFS and Fourier transformed XAFS spectra for the ground state and the laser-excited $[Cu^{I}(dmp)_2]^+$. The Cu−N peak in Figure 6B for the laser excited $[Cu^{I}(dmp)_2]^+$ is higher and shifted to a shorter distance compared to the ground state, suggesting an increase in the coordination number of copper and the decrease of the average Cu−N distance. Table 2 lists the structural parameters for the nearest neighboring shell from the XAFS analysis. An average Cu−N distance of 2.07 Å and a coordination number of four for the ground state $[Cu^{I}(dmp)_2]^+$ were used as reference based on the crystal structure of $[Cu^{I}(dmp)_2]NO_3$,[57,66] although the structure of $[Cu^{I}(dmp)_2]^+$ in solution may deviate from the crystal structure. For our purpose of finding the structural differences between the ground and the MLCT states, these assignments were adequate. The average Cu−N distance for the laser-excited sample fit to two distances of 2.07 and 2.03 Å, respectively, judged by the fitting residual reduction in the two-distance model by a factor of larger than three compared

(83) Kau, L.-S.; Spira-Solomon, D. J.; Penner-Hahn, J. E.; Hodgson, K. O.; Solomon, E. I. *J. Am. Chem. Soc.* **1987**, *109*, 6433−6442.
(84) Smith, T. A.; Penner-Hahn, J. E.; Berding, M. A.; Doniach, S.; Hodgson, K. O. *J. Am. Chem. Soc.* **1985**, *107*, 5945−5955.

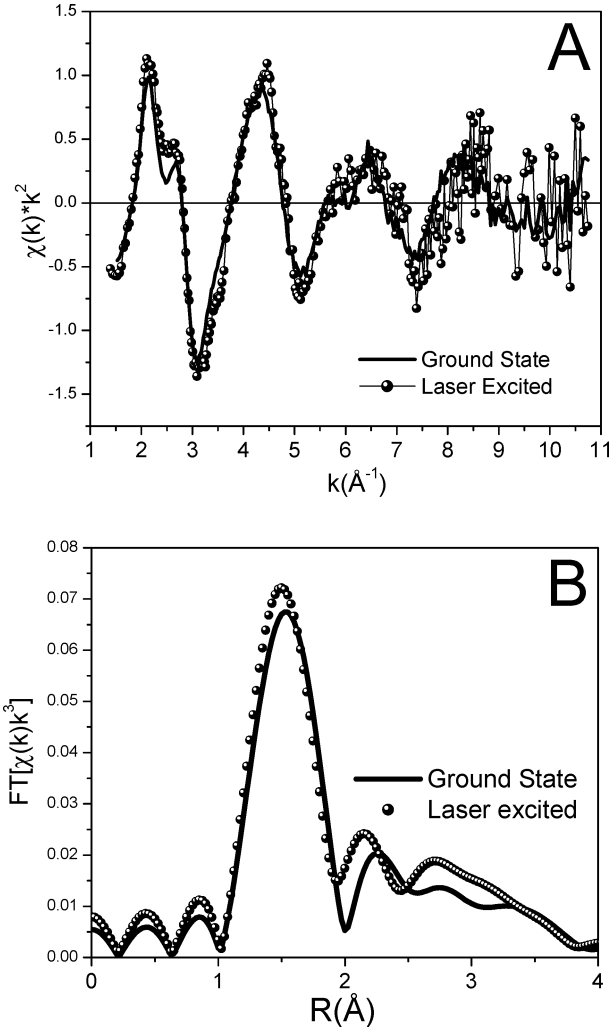

Figure 6. (A) XAFS and (B) the Fourier Transform XAFS spectra of the ground state and the laser excited $[Cu^I(dmp)_2]^+$ in acetonitrile.

Table 2. Ground and MLCT State $Cu^I(dmp)_2^+$ Structures[a]

	coord num	R(Å)[c]	σ^2(Å^2)[d]	residuals
ground-state $Cu^I(dmp)_2^{+b}$	4.0 ± 0.5	2.07 ± 0.02	0.0009	
laser excited (fit 1 bond length)[b]	4.4 ± 0.5	2.05 ± 0.02	0.0004	3.7
laser excited (fit 2 bond lengths)[e]	4.6 ± 0.5 (80%) 5.0 ± 1.0 (20%)	2.07 ± 0.02 2.03 ± 0.04	0.0060 −0.007	1.0

[a] Only the nearest neighboring atomic shell is presented. [b] Using $Cu^I(dmp)_2NO_3$ solid as reference, with an average Cu−N distance of 2.07 Å and a coordination number of 4. More recent crystallographic data indicated shorter Cu−N distances of 2.03 Å. However, the different references will affect the results on the Cu−N bond distance change between the ground and the MLCT states. [c] Cu−N bond distance. [d] Debye−Waller factors. [e] Using $Cu^I(dmp)_2NO_3$ for both shells.

to the one-distance model. Clearly, the first Cu−N distance is from the ground state, and the second is from the MLCT state. Although XAFS spectra routinely resolve bond distance difference of 0.02 Å, a 0.04 Å error is estimated in the average nearest neighbor distance for the MLCT state, due to its relatively small fraction (20%) and the signal-to-noise level of the data. However, the peak shift in the FT-XAFS spectra in Figure 6B clearly indicates that the average nearest neighbor distance of the MLCT state is shorter than that of the ground state. In particular, when the ground state spectrum taken simultaneously with the excited state is used as the reference, the difference between the two states in the average nearest neighbor distances can be resolved more precisely than the error. Because of the error of 10−20% for the coordination number determination by XAFS analyses, it is difficult to confirm the coordination status in the MLCT state from the analysis alone. The more dependable evidence for the pentacoordinated copper in the MLCT state is from the XANES features of the MLCT state described above and the increase of the Cu−N peak height in Figure 6B.

The Ground and the MLCT State Structures of $[Cu^I(dmp)_2]^+$ by DFT Calculations. *Geometry of the Ground State $[Cu^I(dmp)_2]^+$.* A survey of X-ray structures of $[Cu^I(dmp)_2]^+$ indicates that the cation is distorted from the perfect D_{2d} symmetry.[66,85−88,104] Because the angle between ligand planes is closer to 80° rather than the 90° imposed in D_{2d}, the symmetry is lowered to D_2. Other deviations from D_{2d} include different metal-nitrogen bond lengths for the same ligand. In the interest of computational time, the optimization of the ground-state structure was performed with the constraints of the D_2 point group. Selected optimized structural parameters are presented in Table 3. A three-dimensional view of the ground-state structure optimized in the D_2 point group is shown in Figure 7A. The DFT calculation of the ground state of $[Cu^I(dmp)_2]^+$ structure confirms that the cation is distorted from the D_{2d} symmetry but the distortion from the perpendicular orientation of the ligands is less than 1°, with the dihedral angle between the ligand planes being 89.3° rather than 90.0°. The two Cu−N bonds to each ligand are equivalent because of the D_2 symmetry, but the values of the inter-ligand N−Cu−N angles are slightly different at 124.2° and 125.0°. Changing the symmetry from D_2 to C_{2v} hardly affects the geometry of the complex or the energy (ΔE is 0.0003 au), even though in C_{2v}, the ligand planes are restricted to be perpendicular to each other (Table 3).

Geometry of the Flattened MLCT State of $[Cu^I(dmp)_2]^+$. Initially the optimization of the excited triplet state was done in the D_2 point group, corresponding to vertical excitation. However, this symmetry-restricted state converged to only 10^{-2} Hartree/Å in the gradients, and convergence to stricter limits was unsuccessful. This was due to fluctuations and fractional occupancy of the unpaired electron between the closely spaced (−6.9373 eV and −6.9367 eV) ground-state LUMO and LUMO+1 molecular orbitals during the convergence process.

To obtain geometry of the relaxed excited state, the symmetry of the cation was lowered to C_1. The optimization without any symmetry constraints only converged to 10^{-3} H/Å. The Cu−N bonds were shortened by 0.04 Å upon excitation. As the molecule distorted toward a flatter configuration, the angle between the ligand planes reduced from 89.3° in the ground state to 58.5° in the excited state. The flattening is accompanied by slight rocking of one of the ligands. The energy of the triplet excited state is 1.90 eV higher that of the ground state. The C(N)−C(N) bonds are shortened by 0.02 Å, while the N−C bonds in the diimine fragment become longer by 0.01 Å in the excited state. The geometry of the C_1 excited state (see

(85) Blake, A. J.; Hill, S. J.; Hubberstey, P.; Li, W.-S. *J. Chem. Soc., Dalton Trans.* **1998**, 909−915.
(86) Dobson, J. F.; Green, B. E.; Healy, P. C.; Kennard, C. H. L.; Pakawatchai, C.; White, A. H. *Austr. J. Chem.* **1984**, *37*, 649−659.
(87) Hoffmann, S. K.; Corvan, P. J.; Singh, P.; Sethulekshmi, C. N.; Metzger, R. M.; Hatfield, W. E. *J. Am. Chem. Soc.* **1983**, *105*, 4608−4617.
(88) Dessy, G.; Fares, V. *Cryst. Struct. Commun.* **1979**, *8*, 507−510.

Table 3. Theoretical Optimized Geometries of the Ground-State and Excited-Triplet-State of $[Cu(dmp)_2]^+$ and Experimental Ground State Values Averaged over $[Cu^I(dmp)_2]^+$ Salts

	GS[c] experiment[a]	GS[c]	GS[c]	ES$_{tr}$[d]	ES$_{tr}$(NCH)[e]	GS[f] Cu^{II}
point group		D_2	C_{2v}	C_1	C_1	C_1
Cu−N	2.013 (0.012) 2.032 (0.014) 2.041 (0.013) 2.070 (0.030)	2.031	2.033	1.985; 1.998 1.989; 1.996	1.992; 2.010 1.989; 2.011	2.003; 2.021 2.005; 2.019
∠N−Cu−N						
ligand 1	82.12 (0.523)	82.2	82.1	83.6	83.3	83.1
ligand 2	82.39 (0.573)		82.1	83.7	83.3	83.1
flattening angle[b]	84.27 (3.37)	89.3	90.0	58.5	56.5	65.2
Cu−NCH					3.045	
E$_{bonding}$, eV		−378.9559	−378.9483	−377.0578	−397.3438	−368.1401

[a] Parameters averaged over 10 liquid-nitrogen temperature crystal structures of different salts (Gembicky, M., Kovalevsky, A., Coppens, P. to be published). Values in brackets are root mean-square deviations among the corresponding values in the set of structures. Experimental standard deviations are ∼0.002 Å for distances and 0.04−0.12° for the angles. [b] Angle between NCuN planes defined according to reference 86. [c] Ground state of $[Cu^I(dmp)_2]^+$. [d] Excited triplet state of $[Cu^I(dmp)_2]^+$. [e] Excited triplet state of $[Cu^I(dmp)_2(NCH)]^+$. [f] Ground state of $[Cu^{II}(dmp)_2]^{2+}$.

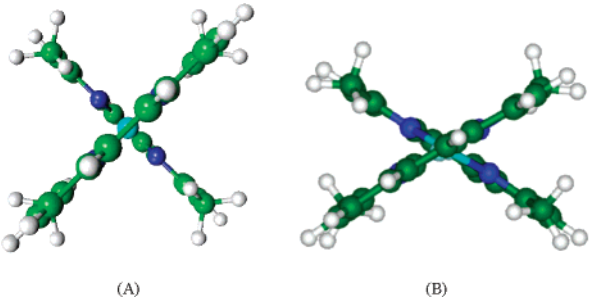

Figure 7. Three-dimensional view of the calculated ground state (A) and the flattened MLCT state (B) of $[Cu^I(dmp)_2]^+$.

Table 4. Hirshfeld Charges

	GS	ES$_{tr}$	Δ(ES$_{tr}$ − GS)	ES$_{tr}$(NCH)
Cu	0.311	0.464	+0.153	0.472
N	−0.119	−0.126	−0.007	−0.120; −0.125
C$_N$	0.040	0.028	−0.012	0.029, −0.030
C$_{N(CH3)}$	0.079	0.077	−0.002	0.076; 0.076
N$_{CH}$				−0.142

Table 5. Mulliken Charges

	GS	ES$_{tr}$	Δ(ES$_{tr}$ − GS)	ES$_{tr}$(NCH)
Cu	0.395	0.648	+0.253	0.674
N	−0.672	−0.706	−0.034	−0.712, −0.716
C$_N$	0.286	0.279	−0.007	0.281, 0.282
C$_{N(CH3)}$	0.206	0.198	−0.008	0.189, 0.182
N$_{CH}$				−0.586

Figure 7B) resembles that of the calculated ground state of $[Cu^{II}(dmp)_2]^{2+}$, which has a flattened geometry with dihedral angle between two dmp planes ∼65° and Cu−N bonds ∼2.00 Å. The Hirshfeld and Mulliken charges (Tables 4 and 5) indicate the copper atom to become more positive upon excitation by 0.15 e and 0.25 e, respectively. As may be expected, this change is much less than the difference between the formal charges of Cu^I and Cu^{II} but in agreement with the charge that resides on Cu in $[Cu^{II}(dmp)_2]^{2+}$ from a separate calculation.

Molecular Orbitals. The ordering of the molecular orbitals in the ground and excited states is presented in Figure 8. The HOMO and HOMO-1 orbitals are very close in energy and would be degenerate e orbitals in the D_{2d} symmetry. These are nonbonding molecular orbitals of mainly metal-centered d_{xz} (HOMO-1) and d_{yz} (HOMO). Similarly the LUMO and

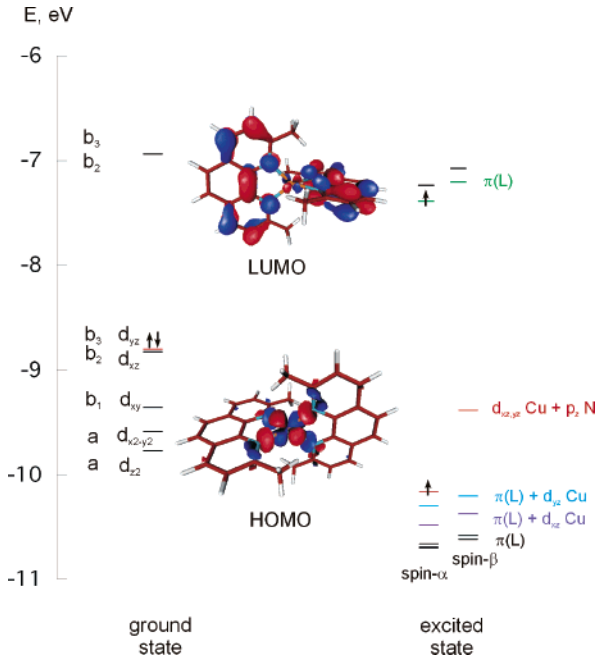

Figure 8. Molecular orbital ordering of the ground and excited triplet states of $[Cu^I(dmp)]^+$. In the ground state, plotted isosurface value 0.035 au; D_2 designations are used to identify the molecular orbitals. The arrows indicate the electron population of the highest occupied orbitals in each case.

LUMO+1 levels are also D_{2d} degenerate e orbitals primarily of ligand-based π-character with some metal $d_{xz,yz}$ contribution. These orbitals correspond to a bonding interaction among the atoms of the ligand, but they are antibonding in the metal region. In the flattened MLCT state, the former ground-state HOMO and the orbitals just below acquire significant ligand π-character, and the contribution of the metal orbitals diminishes. The HOMO−LUMO gap of the ground state is 1.86 eV. In the flattened MLCT state, the separation of the now singly occupied (spin α) orbitals increases to 2.78 eV. This value is quite similar to the HOMO−LUMO gap (2.70 eV) obtained in a separate calculation of the Cu(^{II}) ground state.

Geometry of Ligated MLCT State of $[Cu^I(dmp)_2]^+$ with a Fifth Ligand. To investigate the exciplex formation evident from the XAFS work, geometry optimizations of the HCN adduct of the MLCT state of $[Cu^I(dmp)_2]^+$ were performed without symmetry constraints. The gradient convergence criterion was set to 10^{-3}

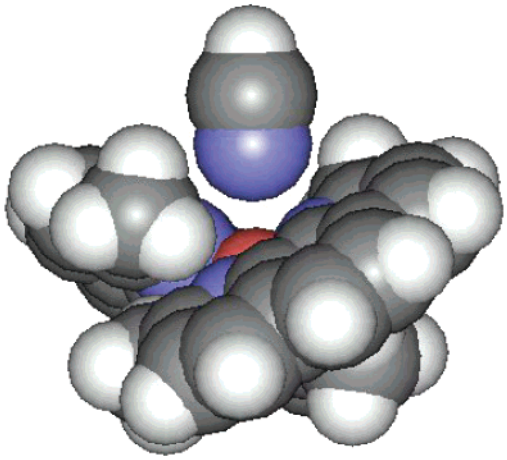

Figure 9. Space-filling model of $[Cu(dmp)_2(HCN)]^+$. (van der Waals radii: Cu 1.15 Å, N 1.40 Å, C 1.55 Å, H 1.10 Å).

Hartree/Å as in the case of optimized flattened MLCT state of $[Cu^I(dmp)_2]^+$. The structural parameters are presented in Table 3. Upon coordination of the HCN ligand, the Cu−N bonds lengthened by about 0.01 Å compared to the flattened MLCT state, while other bonds did not change significantly. The interligand angle decreases upon introduction of the axial ligand, from 58.5° in the four-coordinate triplet state to 56.5°, corresponding to a further flattening for the pentacoordinated complex. However, HCN approaches the copper center only to 3.05 Å. From the CPK (space-filling) models of this complex (Figure 9), it appears that steric hindrance prevents a closer approach to the copper center.

Excited-State Transition Energies as a Function of the Flattening. To obtain an estimate of the spectral shift on flattening of the MLCT state, energy differences between the triplet states in different geometries were calculated by the TD-DFT method, following a procedure outlined by Ricciardi et al.[76b] TD-DFT calculations of singlet−triplet excitations were carried out for geometries at intervals of 10 degrees along the dihedral distortion angle. The spacing between the two triplet levels at each of the geometries along the flattening coordinate is then obtained as the difference between the corresponding singlet−triplet transitions. Figure 10 shows the energies of the symmetry-allowed triplet−triplet transitions in 400−750 nm region. In the D_2 symmetry notation, they are the $^3(B_1,B_2,B_3)\leftarrow{}^3A$, $^3(A,B_2,B_3)\leftarrow{}^3B_1$, $^3(A,B_1,B_3)\leftarrow{}^3B_2$, and $^3(A,B_1,B_2)\leftarrow{}^3B_3$ transitions. The lowest triplet level of A symmetry (point group D_2) is considerably stabilized on flattening, while the higher levels are progressively less stabilized or destabilized, thus predicting the occurrence of a blue shift in the triplet-state absorption spectrum upon relaxation of the excited state. The higher triplet levels with the appropriate energy to account for the observed transient state absorption from the A state of about 550 nm are of B_1, B_2, and B_3 symmetry. All curves of excited state transition wavelength vs the dihedral angle between the two dmp planes follow the same trend, indicating that the flattening of the tetrahedral coordination in the MLCT state may be at least partially responsible for the blue shift in EA during 10−20 ps after the photoexcitation.

Discussion

Dynamics of Photoinduced Structural Rearrangements in the MLCT State of $[Cu^I(dmp)_2]^+$. As observed by the pump−probe XANES and XAFS measurements, molecular structural rearrangements in the F−C MLCT state of $[Cu^I(dmp)_2]^+$ transforms the tetrahedral coordination of Cu^I into a pentacoordinated Cu^{II}*, but the dynamics of this photoinduced transformation have been sparsely investigated. Four events are

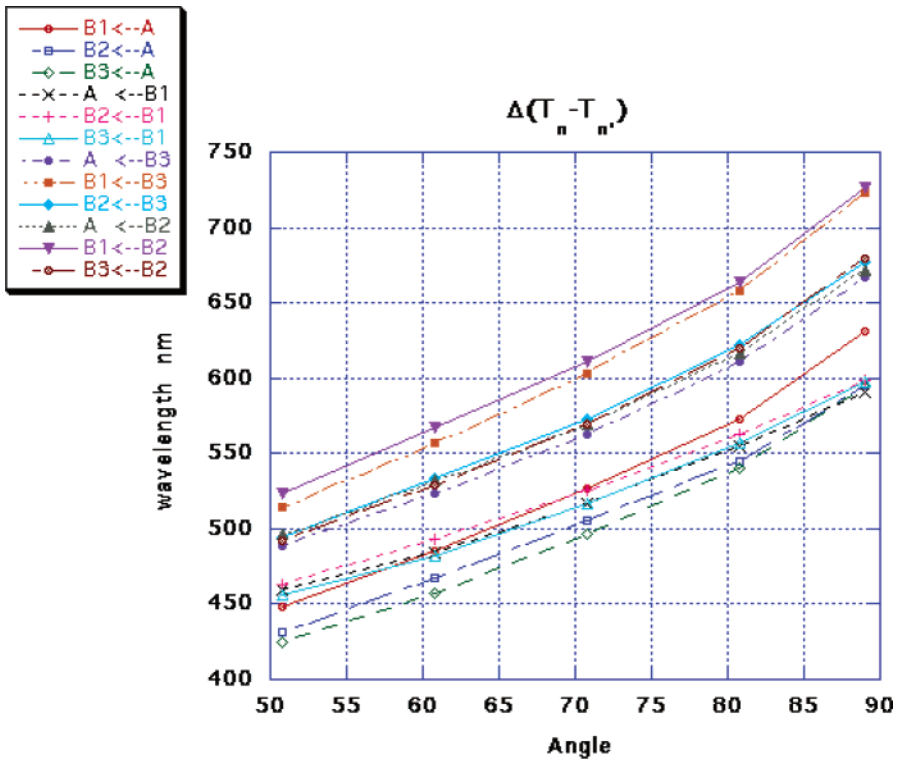

Figure 10. The calculated wavelengths (in nm) for symmetry-allowed triplet−triplet excitations (point group D_2, symmetry species A, B_1, B_2, B_3) as a function of the dihedral angle between the dmp planes.

Scheme 2

$$[Cu^{I}(dmp)_2]^+ + h\nu \rightarrow [Cu^{II}(dmp)(dmp)^{\bullet-}]^{+*}\ (FC) \quad (1)$$

$$[Cu^{II}(dmp)(dmp)^{\bullet-}]^{+*}\ (FC) \rightarrow [Cu^{II}(dmp)(dmp)^{\bullet-}]^{+*}\ (flattened) \quad (2)$$

$$[Cu^{II}(dmp)(dmp)^{\bullet-}]^{+*}(flattened) + Q \rightarrow [Cu^{II}(dmp)(dmp)^{\bullet-}Q]^{+*}(ligated) \quad (3)$$

$$[Cu^{II}(dmp)(dmp)^{\bullet-}Q]^{+*}\ (ligated) \rightarrow [Cu^{I}(dmp)_2]^+ + Q \quad \text{or} \quad (4)$$

$$[Cu^{II}(dmp)(dmp)^{\bullet-}]^{+*}(flattened) \rightarrow [Cu^{I}(dmp)_2]^+$$

likely to occur after the photoexcitation: (1) intramolecular charge separation to yield an excited state that is formally Cu^{II}* in the ground-state geometry, the F−C MLCT state, (2) Jahn−Teller distortion to produce a flattened tetrahedral geometry, the flattened MLCT state, and (3) the coordination of a solvent molecule to yield a five-coordinate compound, the ligated MLCT state, and (4) the flattened or ligated MLCT state decays to the ground state. These photoinduced processes are depicted in Scheme 2, where Q is either a solvent molecule or a counterion that binds the Cu^{II}*.[42,43,48,50,54]

Considering the spectral overlap of the intermediates appearing in Scheme 2 and the uncertainty of their spectral properties, it is very challenging to definitively assign the intermediates, their kinetics, or the precise reaction mechanism. Insight can be gained by comparing our results with recent ultrafast investigations of the MLCT excited states of $[Ru(bpy)_3]^{2+}$, a compound with similar diimine ligands and UV−Vis spectral properties but without the significant photoinduced geometry and coordination number changes. Femtosecond studies of $[Ru(bpy)_3]^{2+}$ in acetonitrile showed sub-picosecond time constants for evolution to the ^{3}MLCT state without the appearance of other distinct states.[89,90] A similar time constant might be expected for photoexcited $[Cu^{I}(dmp)_2]^+$ in acetonitrile. Meanwhile, Jahn−Teller effects such as flattening the tetrahedral coordination geometry in the F−C MLCT state (reaction in Scheme 2) and binding the fifth ligand (reaction in Scheme 2) could be cooperative processes occurring on very different time scales.

The ultrafast dynamics data reported here show evidence for at least two distinct transient excited states in addition to the F−C MLCT state. The lifetime of the longest-lived component is 1.5−1.7 ns, which agrees well with the 2-ns lifetime previously reported for the exciplex state $[Cu^{II}(dmp)(dmp)^{\bullet-}Q]^{+}$* in acetonitrile[48] and is therefore reasonably assigned to the ligated MLCT state. However, the evolution from the F−C MLCT state within the first picosecond to a few tens of picoseconds has not been reported previously. A 480 fs rise time in the GB kinetics at 475 nm (Figure 3A) and a 760 fs rise time in the EA kinetics at 600 nm (Figure 3G) likely reflect the formation of the ^{3}MLCT state from the F−C state, which is slightly slower than $[Ru(bpy)_3]^{2+}$.[89,90] Because of the spectral overlap between the GB and EA regions, the sub-picosecond bleaching and rise components in the region between 540 and 560 nm were small and nearly equal, and thus almost canceled out each other. Therefore, by analogy to $[Ru(bpy)_3]^{2+}$, the 500−760 fs components in the $[Cu^{I}(dmp)_2]^+$ ground state bleaching and the excited state absorption can be assigned plausibly to the initial formation of the ^{3}MLCT state.

In contrast to $[Ru(bpy)_3]^{2+}$, which undergoes no significant structural change in the MLCT state, there exists compelling evidence that the tetrahedral geometry of the initially formed $[Cu^{II}(dmp)(dmp)^{\bullet-}]^{+}$* in acetonitrile is transformed via Jahn−Teller distortion to a flattened tetrahedral geometry with an increased coordination number (reactions 2 and 3 in Scheme 2). The fs transient optical absorption data reported here provide new clues into the dynamics of these Jahn−Teller effects. Although a definitive assignment of the 10−20 ps time constant was difficult due to uncertainties in the optical responses as functions of the excited state structure, this component is likely related to reactions 2 and 3 in Scheme 2 after the assignments of the sub-picosecond and the nanosecond components mentioned above.

The other possible process accompanying the structural changes in reactions 2 and 3 may be vibrational cooling, which has been diagnosed with spectral narrowing and blue shift.[91] The same symptoms in Figure 2B within 10−20 ps after the photoexcitation bear similarities to those observed in t-stilbene,[91,92] where both vibrational cooling and the structural changes were present. Our initial hypothesis was that the optical absorption of the MLCT state could also be a function of the dihedral angle between the two dmp planes or could vary with the ligation. However, judging by the invariance of the "double-hump" feature in different solvents, ranging from those forming the exciplex to those only weakly interacting with the Cu(II)*, the spectral changes within 10−20 ps after the photoexcitation were probably not due to the ligation of the fifth ligand.

To explore the validity of our the hypothesis, DFT calculations were performed. A previous calculation indicated that the energy gap between the HOMO and LUMO in the ground state of a model compound for $[Cu^{I}(dmp)_2]^+$ decreased with the dihedral angle between the two ligand planes due to simultaneous increase and decrease of the HOMO and LUMO energies, respectively.[40] The LUMO energy decrease with the flattening of the tetrahedral geometry could result in a simultaneous decrease in the lowest excited state energy, because the HOMO to LUMO transition generally dominates the lowest energy transition. The most convincing evidence for the correlation between the flattening of the tetrahedral coordination and the blue shift in the EA spectra is from the TD-DFT calculations on the energies for the transitions $T_n \rightarrow T_{n'}$ as a function of the dihedral angle between the two dmp planes shown in Figure 10. Apparently, the energy differences between the lowest and upper triplet levels with the proper spacing to generate EA in 500−600 nm region all follow the same trend, with the smaller dihedral angle associated with the larger transition energy, implying a blue shift in EA spectra due to the flattening of the tetrahedral coordination within 10−20 ps after the photoexcitation.

Alternatively, the two fast time constants could result from biphasic structural reorganization in the MLCT state, where the sub-ps time constant corresponds to the initial structural change that may include the ligation with a solvent molecule accidentally located in the vicinity and with the correct orientation, and the 10−20 ps time constant is due to further structural stabilization of the exciplex with the fifth ligand. However, the

(89) Damrauer, N. H.; Cerullo, G.; Yeh, A.; Boussie, T. R.; Shank, C. V.; McCusker, J. K. *Science* **1997**, *275*, 54−57.
(90) Yeh, A.; Shank, C. V.; McCusker, J. K. *Science* **2000**, *289*, 935−938.
(91) Tan, X.; Gustafson, T. L.; Lufumeux, C.; Burdzinski, G.; Buntinx, G.; Piozat, O. *J. Phys. Chem. A* **2002**, *106*, 3592−3598.
(92) Kovalenko, S. A.; Schanz, R.; Hennig, H.; Ernsting, N. P. *J. Chem. Phys.* **2001**, *115*, 3256−3273.

molecular motion that reduces the dihedral angle between the two dmp ligands, or the flattening of the tetrahedral geometry, is prerequisite for binding the fifth ligand and resembles those internal rotations of an aryl group with a similar size as the dmp group in twisted intramolecular charge transfer (TICT) processes,[93] which takes place in about 15 ps. To stabilize the ligation with acetonitrile ligand, similar motions that contribute to the flattening of the tetrahedral geometry formed by the dmp ligands and the diffusive motion of the acetonitrile must be cooperative, and such motions are likely to take place within 10−20 ps rather than sub-ps.

The Structure of Ligated MLCT State, the Exciplex, and Its Implications. The important structural features of the MLCT state are the oxidation state, coordination number, and geometry of the Cu^{II}* center. As seen from the MO energy level diagram in Figure 8, the HOMO and HOMO − 1 mainly consist of Cu $3d_{xz}$ and $3d_{yz}$ orbitals, while the LUMO and LUMO + 1 have major contribution from the ligand π orbitals. The lowest energy photoexcitation is generally dominated by the HOMO → LUMO transition that depletes electron density from the Cu^{I} 3d orbitals. Therefore, the copper oxidation state at the MLCT state is nominally Cu^{II}*. Because of the intramolecular charge separation resulting from the MLCT transition, the apparent oxidation state of the Cu^{II}* center will differ from that of the ground-state Cu^{I} center by, nominally, one whole charge. However, the DFT calculations obtained the charge shift (0.25e) from Cu to the ligand in the flattened MLCT state, similar to the charge difference between the $[Cu^{I}(dmp)_2]^+$ and $[Cu^{II}(dmp)_2]^{2+}$ ground states. Therefore, this is in agreement with identical positions of the Cu K-edges of the ground state $[Cu^{II}(dmp)_2]^{2+}$ and the Cu^{II}* center in the MLCT state of $[Cu^{I}(dmp)_2]^+$.

The coordination geometry of the Cu^{II}* center in the MLCT excited state is very important in revealing the structural factors controlling the excited-state properties, such as lifetimes and luminescence quantum yields. According to extensive studies in the literature, it is the formation of the exciplex between the Cu^{II}* center in the MLCT state of $[Cu^{I}(dmp)_2]^+$ with a Lewis basic solvent molecule that causes the excited-state quenching. The mechanistic aspect of the atomic motions associated with the Jahn−Teller distortion and formation of the exciplex is responsible for enabling the functional groups in molecular shuttles and switches in previous studies.[26] The XANES evidence from this study supports the ligation of the Cu^{II}* center with an additional fifth ligand, as seen in Figure 5. The most pronounced evidence is an attenuation of the distinctive shoulder feature at 8.985 keV upon the laser excitation. This shoulder feature was assigned to the 1s → $4p_z$ transition when the $4p_z$ is localized on the copper with a square-planar or tetrahedral geometry.[83,84] When the fifth and the sixth ligands bind to the metal along the z direction, the $4p_z$ orbital was delocalized, and the sharp peak due to the 1s → $4p_z$ transition was broadened and appeared to be smoothed.[83,84] Such changes in XANES spectra of transition metal complexes due to the ligation have been observed in metalloporphyrins with and without one or two axial ligands,[16,94−96] as well as in other transition metal complexes.[14,83,84,97,98] Therefore, the smooth transition edge in the XANES spectrum of the MLCT state in Figure 5B strongly suggests a penta- or hexa-coordination geometry of the copper center. However, the steric hindrance from the methyl groups on the 2 and 9 positions of the phenanthroline ligands prohibits the hexa-coordination, and thus the penta-coordination is a preferred geometry for the MLCT state.

An average shortening of 0.04 Å in the Cu−N bonds was clearly visible from the XAFS spectra, as well as from the Fourier transformed XAFS spectra. Compared with the ground-state structure, shorter Cu−N bond lengths were also obtained from the DFT calculations for the flattened and the ligated MLCT states with or without HCN as the fifth ligand (Table 3). Using the ground state $[Cu^{I}(dmp)_2]^+$ spectrum taken simultaneously instead of $[Cu^{II}(dmp)_2]NO_3$ spectrum taken separately as the reference (see Experimental Methods), the data from our previous study in toluene were reanalyzed, resulting in a Cu−N elongation of 0.04 Å instead of 0.07 Å.[14] Despite the evidence in previous excited-state Raman studies on the localization of the excited state on one dmp ligand,[82] we are unable to resolve discrete Cu−N distances from the current experimental X-ray data.

The XANES spectra provided strong evidence for the penta-coordinate Cu^{II}* in both acetonitrile and in toluene (our previous work). These results are in accordance with the fact that Cu^{II}* in the MLCT excited state is formally a 17 electron d^9 system prone to the addition of a fifth ligand.[41] In addition, a photodriven increase in the copper coordination number has previously been invoked to explain the quenching of copper excited states by Lewis bases, forming the exciplex.[41−51,54,99] It is well known that MLCT excited states in general[100,101] follow Jortner's energy gap law that the nonradiative rate constant increases exponentially with decreasing energy separation between the ground state and the excited state.[49,102] The formation of the exciplex stabilizes the MLCT state, reducing the energy gap between the ground state and the MLCT state. As the energy gap becomes small enough, due to the strong interaction of the Cu center with the ligand, the nonradiative decay dominates the relaxation pathway, and no emission is detected (e.g., as in the acetonitrile solution case).

Although the results from the XANES and XAFS for $[Cu^{I}(dmp)_2]^+$ are consistent with the DFT calculations as well as previous studies, the structural origins for solvent dependency of the MLCT state behavior must be explained. The XANES results for $[Cu^{I}(dmp)_2]^+$ in both toluene and acetonitrile solutions support the formation of a penta-coordinated Cu(II)* center in the MLCT state based on the attenuation of the shoulder feature in the transition K-edge of copper in the XANES spectra. While this deduction is still held, a broad range of the Cu-to-ligand bond distances for the fifth ligand could smooth the transition edge as indicated by previous studies on a large number of

(93) Onkelinx, A.; De Schryver, F. C.; Viaene, L.; Van der Auweraer, M.; Iwai, K.; Yamamoto, M.; Ichikawa, M.; Masuhara, H.; Maus, M.; Rettig, W. *J. Am. Chem. Soc.* **1996**, *118*, 2892−2902.
(94) Inamo, M.; Kamiya, N.; Inada, Y.; Nomura, M.; Funahashi, S. *Inorg. Chem.* **2001**, *40*, 5636−5644.
(95) Endregard, M.; Nicholson, D. G.; Abraham, R. J.; Marsden, I.; Beagley, B. *J. Chem. Soc., Faraday Trans.* **1994**, *90*, 2775−2781.
(96) Kau, L. S.; Svastits, E. W.; Dawson, J. H.; Hodgson, K. O. *Inorg. Chem.* **1986**, *25*, 4307−4309.
(97) Koningsberg, D. C.; Prins, R. *X-ray Absorption*: *Principles, Applications, Techniques of EXAFS, SEXAFS and XANES*; John Wiley & Sons: New York, 1988.
(98) Westre, T. E.; Kennepohl, P.; DeWitt, J. G.; Hedman, B.; Hodgson, K. O.; Solomon, E. I. *J. Am. Chem. Soc.* **1997**, *119*, 6297−6314.
(99) McMillin, D. R.; Kirchhoff, J. R.; Goodwin, K. V. *Coord. Chem. Rev.* **1985**, *64*, 83−92.
(100) Kober, E., M.; Caspar, J. V.; Lumpkin, R. S.; Meyer, T. J. *J. Phys. Chem.* **1983**, *87*, 952.
(101) Meyer, T. J. *Acc. Chem. Res.* **1989**, *22*, 163.
(102) Freed, K. F.; Jortner, J. *J. Chem. Phys.* **1970**, *52*, 6272.

copper complexes.[84] The apparent elongation and the shortening of the average Cu−N bond distance for the MLCT state of $[Cu^{I}(dmp)_2]^+$ in toluene from our previous study[14] and in acetonitrile in this study, repectively, signal the difference in the interactions with the fifth ligand. Such variation was also shown by a broad range of the MLCT state lifetimes in various Lewis base solvents with different electron donating capabilities.[50] Toluene (or BArF anion) is bulkier in size and has less electron donating capability compared to acetonitrile; hence, it could only act as the fifth ligand with a longer and less stable bond with the Cu(II)* center in the MLCT state of $[Cu^{I}(dmp)_2]^+$. Consequently, the MLCT state of the $[Cu^{I}(dmp)_2]^+$−toluene complex will not be as stable as the corresponding acetonitrile complex and will not lower the energy of the MLCT state to such an extent that nonradiative decay becomes the sole path for the MLCT state to return to the ground state.

While the XANES evidence confirmed the existence of the fifth ligand in both toluene and acetonitrile in the MLCT state of $[Cu^{I}(dmp)_2]^+$, the XAFS results revealed a difference in the nearest neighbor bond distances of this MLCT state in the two solvents. The comparison between the MLCT state structures in these two solvents supports our hypothesis that the MLCT state of $[Cu^{I}(dmp)_2]^+$ in toluene behaves in a manner similar to that reported previously for sterically bulky copper compounds. The interaction between the MLCT state of $[Cu^{I}(dmp)_2]^+$ with toluene or the BArF anion was so weak that the complex retained room-temperature luminescence and had the rate constant for radiative and nonradiative decays of $k_r = 1.14 \times 10^4\ s^{-1}$ and $k_{nr} = 1.02 \times 10^7\ s^{-1}$, compared to $k_{nr} = 6 \times 10^8\ s^{-1}$ in acetonitrile. Because the fifth ligand coordinates to the Cu^{II}* center in the MLCT state of $[Cu^{I}(dmp)_2]^+$ in both toluene and acetonitrile, whereas only the latter showed excited state quenching, the exciplexes were previously just inferred for cases where strong excited state adducts completely quenched the excited state.

Conclusion

The MLCT excited-state dynamics and structure of $[Cu^{I}(dmp)_2]^+$ in acetonitrile, a Lewis basic solvent, were investigated. The evolution from the initial F−C state to the triplet MLCT state likely takes place within 500 fs, followed by structural relaxation to a flattened tetrahedral Cu^{II}* site and coordination of a fifth ligand derived from solvent or counterion with a time constant of $5-10 \times 10^{10}\ s^{-1}$. The variation of the MLCT state structure in different solvents confirmed that the origin of distinctly different excited state behavior is due to formation of MLCT state-solvent complexes with different electronic interactions. When the interaction is strong, the MLCT state lifetime is shortened significantly and the luminescence is quenched, which has been characterized by the exciplex formation in previous literature. Therefore, the pump−probe XAFS measurements in the time domain provide new insights into the fundamental aspects in the structural factors that may influence photoinduced electron and energy transfer processes. Further studies on the ultrafast dynamics of the $[Cu^{I}(dmp)_2]^+$ MLCT state in different solutions are in process.[103−104]

Acknowledgment. This work is supported by the Division of Chemical Sciences, Office of Basic Energy Sciences, U.S. Department of Energy under contracts W-31-109-Eng-38, DE-GF02-96ER14662 (G. J. M.) and DE-FG02-02ER15372 (P. C.), by the Petroleum Research Fund administered by the American Chemical Society to G. J. M., and in part by NSF Grant CHE9981864 to P. C. The computations were performed on the 64-processor SGI Origin3800, 32-processor Sun Blade 1000 (UltraSparc III) and 48-processor Sun Ultra-5 (UltraSparc IIi) supercomputers at the Center for Computational Research of the State University of New York at Buffalo, which is supported by Grant DBI9871132 from the National Science Foundation. We would like to thank Drs. Wighard Jäger, Mark Beno, Jennifer Linton, and staff members at BESSRC-CAT, Advanced Photon Source, for their technical assistance, and Mr. Joseph Gregar for his help in the glass design of the sample flowing system.

JA0294663

(103) Shaw, G. B.; Meyer, G. J.; Chen, L. X., to be published.
(104) Gembicky, M.; Kovalevsky, A.; Coppens, P., to be published.